 CMC, vol.9, no.3, pp.209-227, 2009

Wavelet-based Inclusion Detection in Cantilever Beams

Zheng Li[1,2] **Wei Zhang**[1] **and Kezhuang Gong**[1]

Abstract: In this paper, continuous wavelet transform has been applied to inclusion detection in cantilever beams. By means of FEM, a cantilever beam with an inclusion is subjected to an impact on its free end, and its stress wave propagation process is calculated. Here, two kinds of inclusions which are distinct in material behavior have been discussed. And we change the inclusion's sizes in the beam and set it in three different positions to simulate some complicated situations. For soft inclusion, the results show that the arrival times of incident and reflective wave are distinguishable by performing Gabor wavelet transform and extracting a proper frequency component from the strain data of two certain points on beam edge. Consequently, the position of inclusion is identified and the size of it is investigated quantitatively by the reflection and transmission ratio. For hard inclusion, an improved method is adopted to amplify the signal-to-noise ratio. The inclusion is located by analysis of the difference between an intact beam and a beam with inclusion. In addition, the corresponding dynamic experiments for both kinds of inclusions are carried out to verify the detection method. The experimental results show that Gabor wavelet transform precisely estimates the location and size of inclusions, and is proved to be an effective method to quantify the inhomogeneity in a beam.

Keywords: Continuous wavelet transform, Gabor wavelet, inclusion detection, cantilever beam.

1 Introduction

Inhomogeneous inclusion in engineering material always decreases the material quality and induces stress concentrations along interfaces practically, leading to the structural deterioration and safety reduction consequently. But, there will be many chances to generate various impurities inevitably during the manufacture, processing and utilizing of structural components, which cannot be estimated in advance.

[1] LTCS & College of Engineering, Peking University, China.
[2] Corresponding author. Fax: +86-10-62751812, E-mail: lizheng@pku.edu.cn

So, how to detect the material purity in a structure and how to identify the inclusion property are all crucial issues in structural health monitoring. Nowadays, there are many kinds of methods used to detect the damage or mechanical degradation in structures, such as Fourier analysis based on vibration [Reddy K.V. and Ganguli R. (2007)] and Lamb wave technique [Tian J., Gabbert U., Berger H. and Su X. (2004)]. And an overview about the computational intelligence methods developed for the structural integrity assessment of aging aircraft structures was summarized by Pidaparti R.M. (2006). In contrast with the damage or crack, wave reflection and transmission become more obscure when an inhomogeneous inclusion exists in structures, because the conclusion is mostly distinct from the structure material in mechanical behavior. Baganas K. and his co-workers (2005) contributed on identification of a spherical inclusion inside a circular cylinder, and Vanaverbeke S. (2003) studied a plate with a thin inclusion by the reflection of a two-dimensional Gaussian ultrasonic beam. And there are some other current NDT methods utilized to identify inclusions [Carreon H. (2007); Brovko A.V., Murphy E.K., Rother M. and Yakovlev H.V.V. (2008)]. But most of these methods are either inconvenient or unsuitable to apply in engineering structures. Therefore, some new methods need urgently to be developed to detect in-situ the material purity and quality in engineering structures.

Now, a new detective method based on the stress wave propagation is provided in this paper. Because of its very good local and self-adaptive time-frequency analytical properties, continuous wavelet transform has been applied in stress wave analysis [Hull A. J., Hurdis D.A. (2003)] and even in crack detection [Tabrez S., Mitra M. and Gopalakrishnan S. (2007); Tian J., Li Z. and Su X., (2003); Li Z., Xia S., Wang J. and Su X. (2006)]. So, here it will be employed to analyze the stress wave signals in cantilever beams for inclusion detection. Firstly, numerical computation will be carried out for the cantilever beam to identify the location of inhomogeneity, where the dynamical strain data will be extracted and analyzed by Gabor wavelet transform. Then, the corresponding dynamic experiments will be performed for PMMA cantilever beams with various inclusions to validate the reliability of the stress wave method based on continuous wavelet transform for inhomogeneous inclusion detection.

2 Continuous wavelet transform

For any square-integrable signal $f(t)$, its continuous wavelet transform is defined in time domain [Mallat S. (1998)]

$$W_f(a,\tau) = \frac{1}{\sqrt{a}} \int_{-\infty}^{+\infty} f(t) \overline{\psi(\frac{t-\tau}{a})} dt \tag{1}$$

where a is the scale parameter and τ is the translation parameter; ψ is a mother wavelet and the bar indicates its complex conjugate. The Fourier transform of mother wavelet, $\hat{\psi}(\omega)$, needs to satisfy its admissibility condition, i.e.

$$\int_{-\infty}^{+\infty} \frac{|\hat{\psi}(\omega)|^2}{|\omega|} d\omega < \infty \tag{2}$$

There are many commonly used wavelet functions, such as Haar wavelet, Mexician Hat wavelet, Morlet wavelet and compactly supported spline wavelet. However, in this paper, Gabor wavelet is adopted to analyze the stress wave signals for its excellent time-frequency analytical properties. Gabor wavelet can be expressed as

$$\psi_G(t) = \frac{1}{\sqrt[4]{\pi}} \sqrt{\frac{\omega_0}{\gamma}} \exp\left[-\frac{(\omega_0/\gamma)^2}{2} t^2\right] \exp(i\omega_0 t) \tag{3}$$

where γ and ω_0 are positive real constant. Its Fourier transform is,

$$\hat{\psi}_G(\omega) = \frac{\sqrt{2\pi}}{\sqrt[4]{\pi}} \sqrt{\frac{\gamma}{\omega_0}} \exp\left[-\frac{(\gamma/\omega_0)^2}{2} (\omega - \omega_0)^2\right] \tag{4}$$

Although Gabor wavelet cannot strictly satisfy the admissibility condition of Eq. (2), it exhibits best time-frequency characteristics according to Heisenberg uncertainty relation [Heisenberg W. (1927)]. In this paper, we choose $\gamma = \pi\sqrt{2/\ln 2}, \omega_0 = 2\pi$, it is regarded to approximately meet the condition.

If a dispersive wave $u(x,t) = \frac{1}{\sqrt{2\pi}} \int_{-\infty}^{+\infty} A(\omega) \exp[i(\omega t - kx)] d\omega$ is considered, its continuous wavelet transform can be obtained from Eq. (1)

$$W_f(a,\tau) = \sqrt{a} \int_{-\infty}^{+\infty} A(\omega) \exp(-ikx + i\omega\tau) \hat{\psi}_G(a\omega) d\omega \tag{5}$$

where the function $\hat{\psi}_G(a\omega)$ is localized around ω=ω_0/a. Meanwhile, $k = k_0 + \frac{1}{c_g}(\omega - \frac{\omega_0}{a})$, when the first-order approximation of $C_g = \frac{d\omega}{dk}$ is adopted around the frequency ω_0/a. So, Eq. (5) can be simplified as

$$|W_f(a,\tau)| = \frac{1}{\sqrt[4]{\pi}\sqrt{a}} \sqrt{\frac{\omega_0}{\gamma}} |A(\frac{\omega_0}{a})| \exp\left[-\frac{(\omega_0/\gamma)^2}{2a^2} (\tau - \frac{x}{c_g})^2\right] \tag{6}$$

It means that for any given scale parameter a, the amplitude of $W_f(a,\tau)$ will reach its maximum value when $\tau = x/c_g$. Therefore, by changing the scale parameter a, the arrival time and amplitude of the dispersive wave at each frequency can be obtained.

3 Cantilever beam with soft inclusion

In this paper, a cantilever beam, as a common structural component, is considered to identify its inside inclusions. Firstly, a kind of soft inclusion is considered to represent the inner infirm part or to express the local area with many tiny cracks or damages. The inhomogeneous beams are made of PMMA with rubber inclusions, where rubber is chosen as soft inclusion to imitate the local area with many tiny damages, as well as other soft inclusions which elastic modulus is normally smaller than matrix materials. The beam is set with 600mm in length, 5mm in thickness and 32mm in width, and its material properties are listed in Table 1.

Table 1: Material properties for soft inclusion beam

Material	PMMA	Rubber
E_d (GPa)	5.03	0.008
ρ (kg/m^3)	1170	912
ν	0.36	0.49

Basically, three kinds of beam models are designed with an inclusion at three different locations as illustrated in Fig. 1, namely, an inner inclusion, an inclusion located on the upper edge and an inclusion on the lower edge. Moreover, the inclusions are designed with different aspect ratios. With the width being fixed to 1mm, the damage length is set to be 3, 6, 9, 12 and 15mm, separately. Two points A and B on the upper edge of cantilever beam as shown in Fig. 1, are chosen to measure the dynamic stain signals during an impact load on the free end of beam.

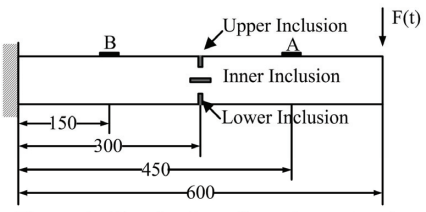

Figure 1: Sketch of cantilevel beam (mm)

3.1 Numerical calculation

Firstly, all models are calculated by ANSYS /LS-DYNA programme. The problem is simplified as a 2D plane-stress state, and 2D PLANE 162 element type is selected to divide finite element model into about 19200 elements. The element size is set

1mm for less than 1/20 of minimum stress wave length to satisfy the calculated precise and time steps are automatically calculated, about 5×10^{-8}s, to achieve convergence. An impact load acts on the free end of beam, and it is introduced by corresponding experiment data in Fig. 2. When the soft inclusion exists on the upper edge of cantilever beam, the longitudinal strain data at points A and point B are calculated. Fig. 3 shows the strain results at points A and B with different inclusion lengths from 0, 3mm to 15 mm, and specimens are nominated as No_inclusion, R1_3 to R1_15 respectively.

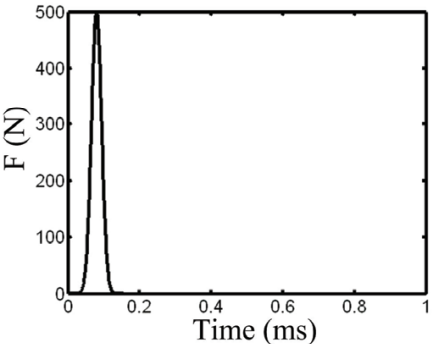

Figure 2: Impact load

From Fig. 3, it can be seen that the strain signals of point A before the first peak look same, and then it will be fluctuated when the inclusion length increases. But the strain signals at point B seem no obvious change in these figures. Therefore, from the data of point A, we can identify whether there are soft inclusions in the beam, but it is difficult to determine the inclusion position directly from these complicated figures due to the dispersive characters of flexural waves.

In order to obtain more information from the strain signals, Gabor continuous wavelet transform (CWT) is employed to analyze these data, but how to choose a proper wavelet parameter is very significant. By changing the analysis frequency from 5 kHz to 30 kHz, the typical CWT results of strain data at points A and B are calculated and shown in Fig. 4. It originally is a 3-D image of time-frequency analysis, where x axis is time, y axis is frequency and z axis is the amplitude of CWT. Now, we look down upon the image from z axis and use different colors to express the CWT amplitudes in brief. According to Timoshenko beam theory, the flexural waves in beams are dispersive, and there are two sets of wave modes, slow wave and fast wave. If the mechanical properties of materials are taken from Table 1, the cut-off value of fast wave can be calculated about 17.3 kHz, and it is apparent in all figures in Fig. 4, even in the No_inclusion beam. Therefore, an attempt is made

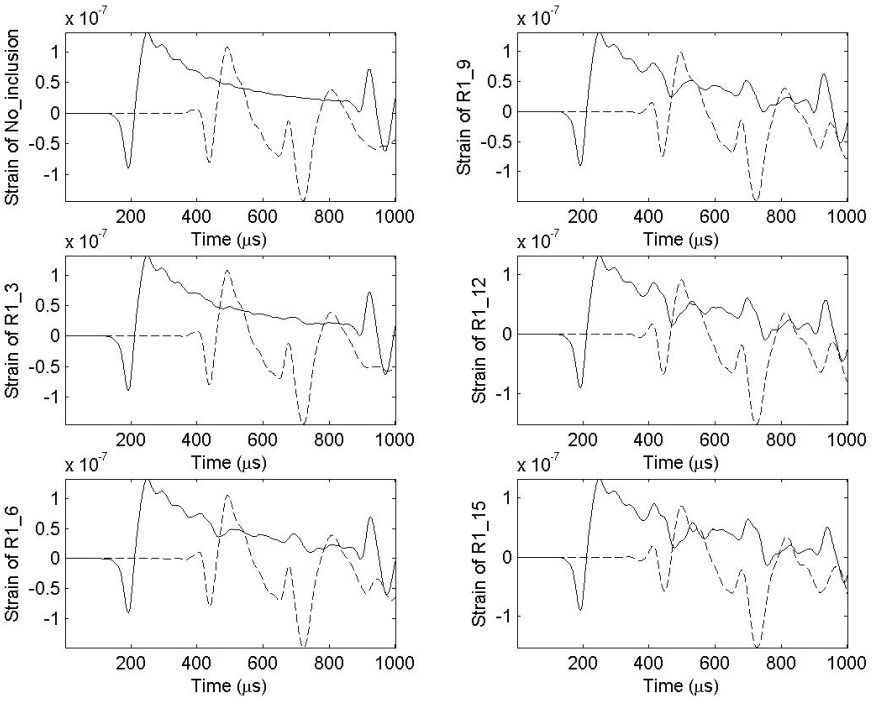

Figure 3: Strain results for upper soft inclusion

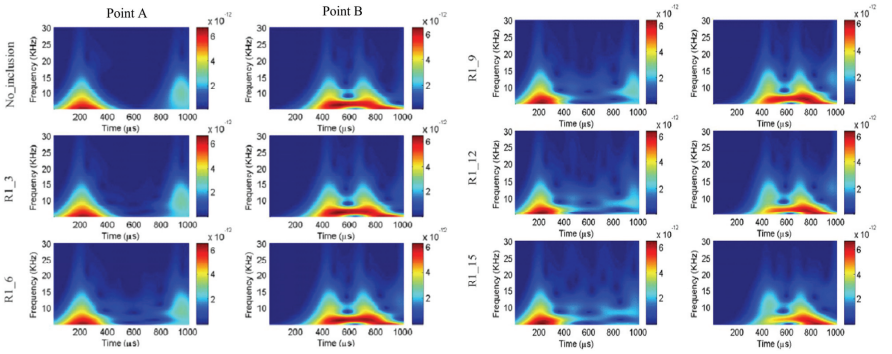

Figure 4: Multi-frequency analysis of CWT for upper soft inclusion

to avoid the influence of fast wave by choosing lower cut-off frequency signals. However, it can be found that the additional ridge reflected by inclusion is difficult to identify from very low frequency results of point A, which contributes to the larger time window at low frequency in wavelet analysis. So, only the middle high

frequency component below the cut-off can be used to detect the inclusion, and it is obviously that the additional ridge can be identified near the frequency of 10.0 kHz. Therefore from the results of multi-frequency CWT analysis, the analysis frequency of CWT can be selected.

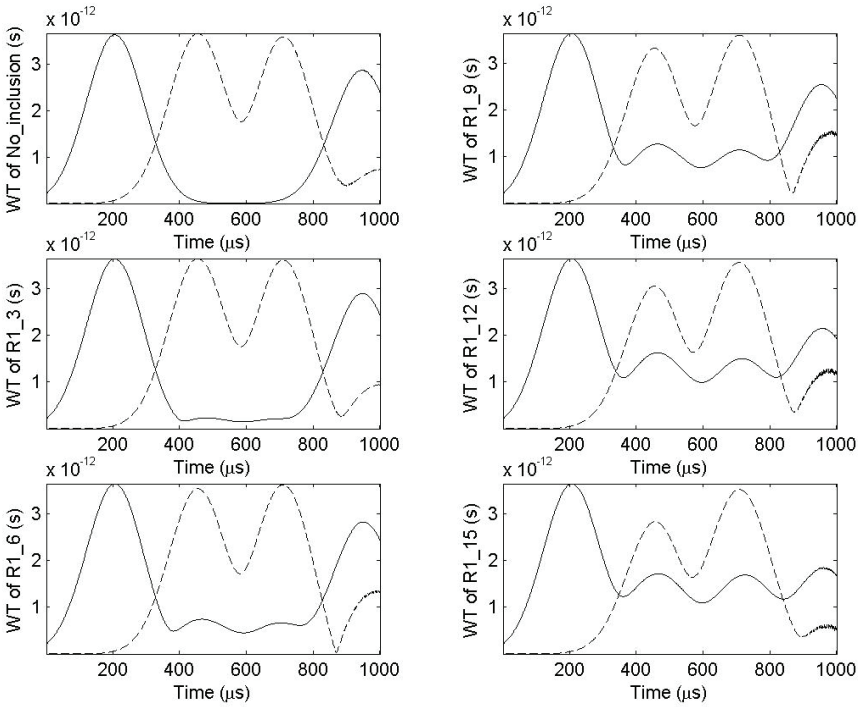

Figure 5: CWT results for upper soft inclusion (10.0 kHz)

Fig. 5 shows the results of Gabor wavelet transform about point A and point B by choosing the analytical frequency in 10.0 kHz. It can be noticed, for the beam with soft inclusion, the first peaks of solid curves (point A) correspond to the arrivals of incident waves, and the second ones represent the arrival of reflected waves. The first peaks of dot curves (point B) correspond to the arrival of transmitted waves. Then, by calculating the stress wave velocity at this frequency components from the distance and arrival times of stress wave at points A and B, the location of inclusion can be easily determined by the difference of the arrival times between incident and reflected waves.

Similarly, the situations with an inner or lower inclusion in the beam can also be calculated and typical results extracted by Gabor wavelet transform are displayed

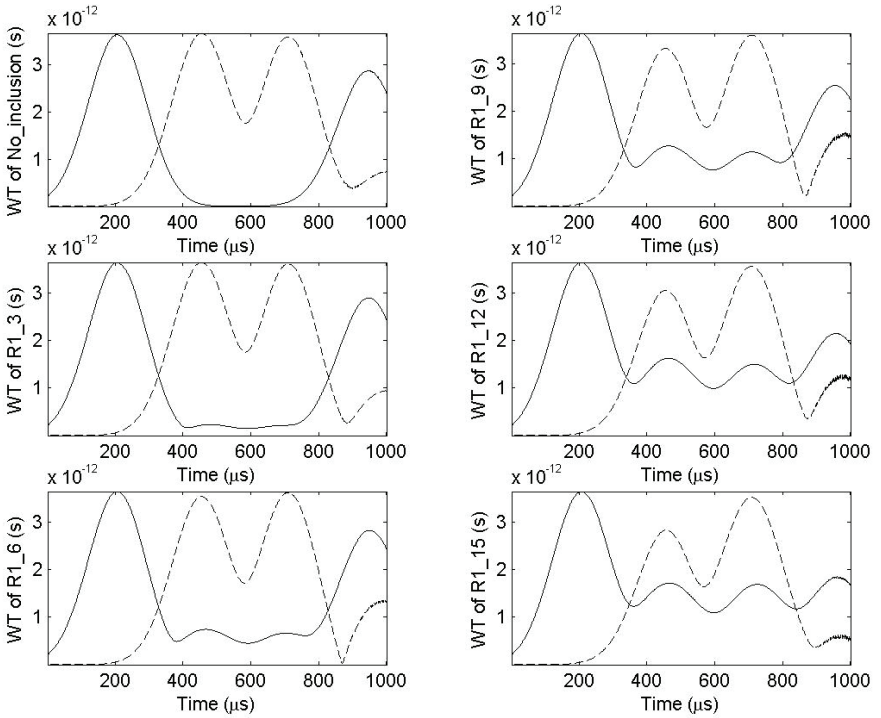

Figure 6: CWT results for inner soft inclusion (12.5 kHz)

in Fig. 6 and Fig. 7, respectively.

To demonstrate the accuracy of inclusion detection, all results about predicted location of inclusion for the three beams are listed in Table 2. It can be noticed when the inclusion depth ratio of the inclusion depth (d) to the beam width (h), is larger than 10%, the detecting error in inclusion location is no more than 5%. When the inclusion is very small (d/h<10%), its location can be also successfully identified, though the error will increase. This indicates that this method is accurate for moderate soft inclusions and has high sensitivity for small ones. Furthermore, Fig. 8 shows the reflection and transmission ratios about different inclusion lengths to compare the influence of inclusion extent. It can be seen that, all reflection ratio curves rise when the inclusion length increases, but contrarily, the transmission ratio curves tend to decline. So, from the results in Fig. 8, the size of soft inclusion can be estimated.

Table 2: Results of soft inclusion

Inclusion Length (mm)	Inclusion Length Ratio d/h (%)	Upper Inclusion		Inner Inclusion		Lower Inclusion	
		Predicted Location (mm)	Error (%)	Predicted Location (mm)	Error (%)	Predicted Location (mm)	Error (%)
3	9	166.3	10.9	153.7	2.5	151.2	0.8
6	19	157.8	5.2	152.5	1.7	153.1	2.0
9	28	154.8	3.2	150.6	0.4	153.7	2.5
12	37	154.8	3.2	149.4	-0.4	153.1	2.1
15	47	154.2	2.8	149.4	-0.4	140.7	-6.2

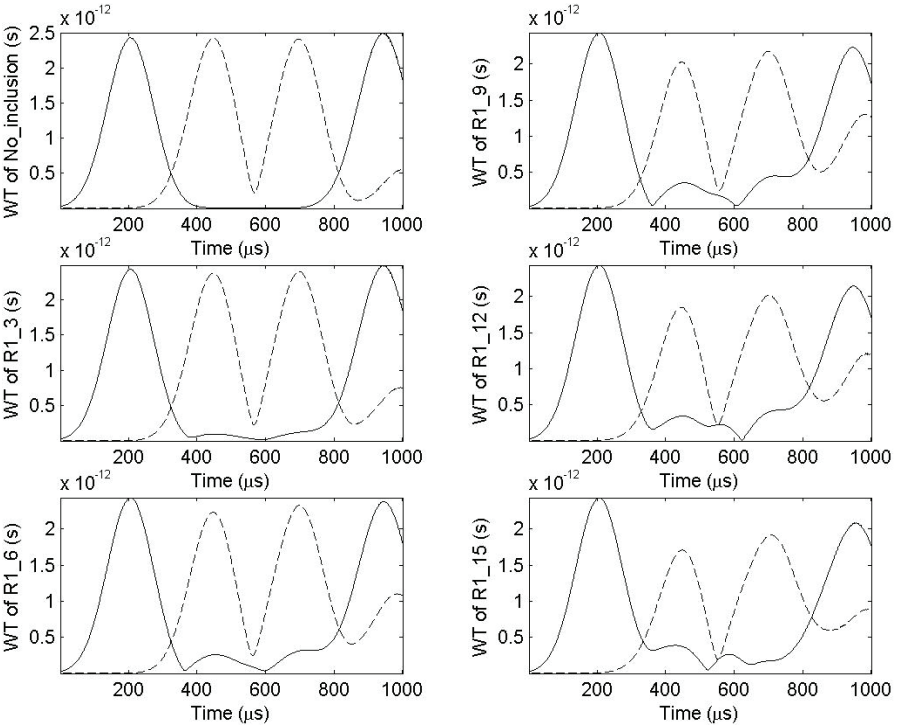

Figure 7: CWT results for lower soft inclusion (13.0 kHz)

3.2 Experiments

Experiments are carried out to directly measure the dynamic strain signals on the edge of beams for the aforementioned beam, and the materials selected are the same as computational models. Here, the PMMA beam with a rubber inclusion on its upper edge is prepared. Two strain gauges at points A and B (see Fig. 1) are glued to measure the strain data, which can be recorded by a two-channel digital oscilloscope (Tektronic2211). The beam is impacted laterally on its free end by a dropping steel ball with 1.2m height. The typical strain signals and CWT results about the beam with an upper rubber inclusion, which is 2mm width and 10mm length, are both illustrated in Fig. 9, where the analysis frequency of 10.0 kHz is chosen. According to these results in Fig. 9, the inclusion location can be identified precisely and the error is about 3.1%. For this case, the reflection and transmission ratios can also be figured out and they are 23% and 73%, respectively. The experimental results in Fig. 9 show great consistency with computational results basing on finite element analysis, and demonstrate that this inclusion detection method is

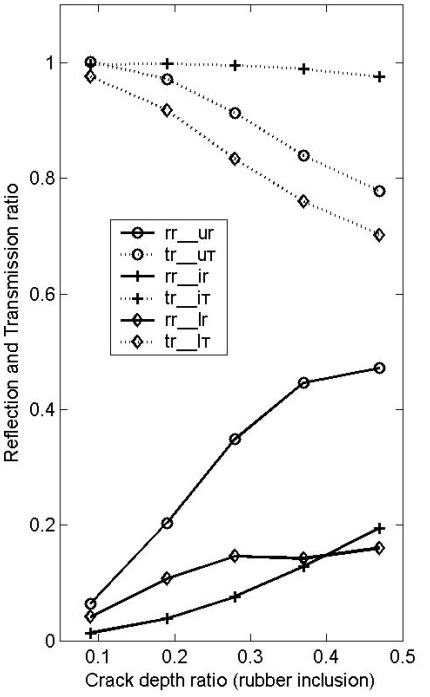

Figure 8: Reflection and transmission ratios

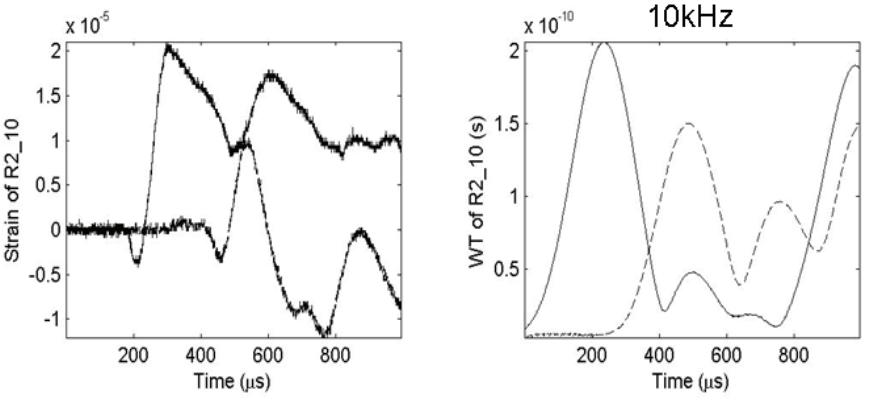

Figure 9: Strain and CWT results of experiment for soft inclusion

remarkably effective and sensitive to soft inclusion in a cantilever beam.

4 Hard inclusion detection

Furthermore, by replacing rubber with steel in Fig. 1, the hard particles included in pure materials are imitated. The mechanical properties of beam and inclusion are shown in Table 3. Similarly, under an impact loading on its free end, the cantilever beam with a steel inclusion is considered, and both numerical calculation and experiments are performed to acquire the dynamic strain data for impurity detection. The hard inclusions are set with 1mm in width but its length can be changed from 0, 3mm to 15mm, and specimens are nominated as No_inclusion, S1_3 to S1_15 respectively.

Table 3: Materials properties for hard inclusion beam

Material	PMMA	Steel
E_d (GPa)	5.03	210
ρ (kg/m^3)	1170	7800
ν	0.36	0.28

4.1 Numerical calculation

Also, all models are calculated by ANSYS /LS-DYNA programme, and Fig. 10 shows the dynamic strain signals on points A and B of beam (see Fig. 1), where solid curves are about point A and dashed curves are about point B. In Fig. 10, it can be noticed that the fluctuation of signal point A is not very obvious when the inclusion size increases, and all signals of point B seem similar. So, it is a little hard to identify the hard inclusion inside directly from strain results. In addition, it can be estimated that the reflected signals from hard inclusion will be very small and the transmitted signals will be disturbed slightly by hard inclusion.

To obtain the analytical frequency of wavelet transform to detect the existence of hard inclusion in beam, a multi-frequency analysis of CWT, from 5Hz to 30 Hz, is performed for the strain results at points A and B, and shown in Fig. 11. But, it can be found that the reflected signals as additional ridges for point A results are much weaker, and only for big hard inclusions the additional ridges can be seen. Therefore, an improved date processing has to be adopted.

In order to amplify the effect of hard inclusions, the difference of strain responses between an inclusion beam and a non-inclusion beam is calculated by CWT and shown in Fig. 12. Fig. 12 shows the multiple frequencies results of point A with the different hard inclusion sizes from 3mm to 15mm, and it can be found that the

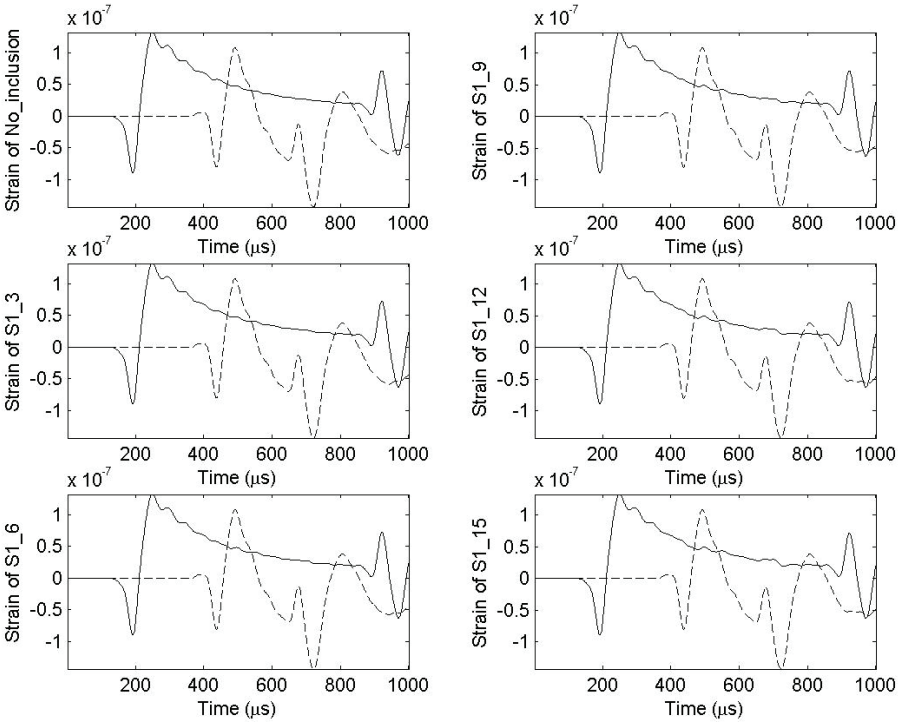

Figure 10: Strain results for upper hard inclusion

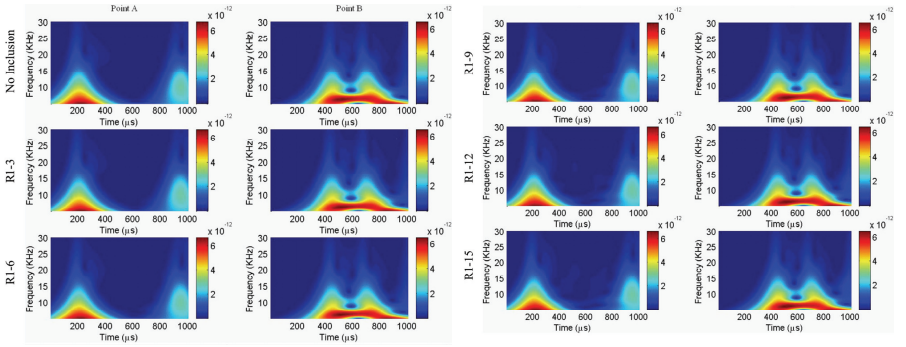

Figure 11: Multi-frequency analysis of CWT for upper hard inclusion

additional ridges are obviously identified. During the components of CWT from 10 kHz to 15 kHz, the reflected signals are easily to be caught and the peaks mostly focus around $450\mu s$. So, the Gabor wavelet transform is employed to extract the component around 11.0 kHz frequency components, and the results are plotted in Fig. 13. In Fig. 13, the first peaks express the difference of incident waves and the second ones are the difference of reflected waves from hard inclusion, so it is apparent that the ratio about the two differences will increase with the increment of inclusion size. Consequently, the inclusion extent can be predicted too by the improved detection method.

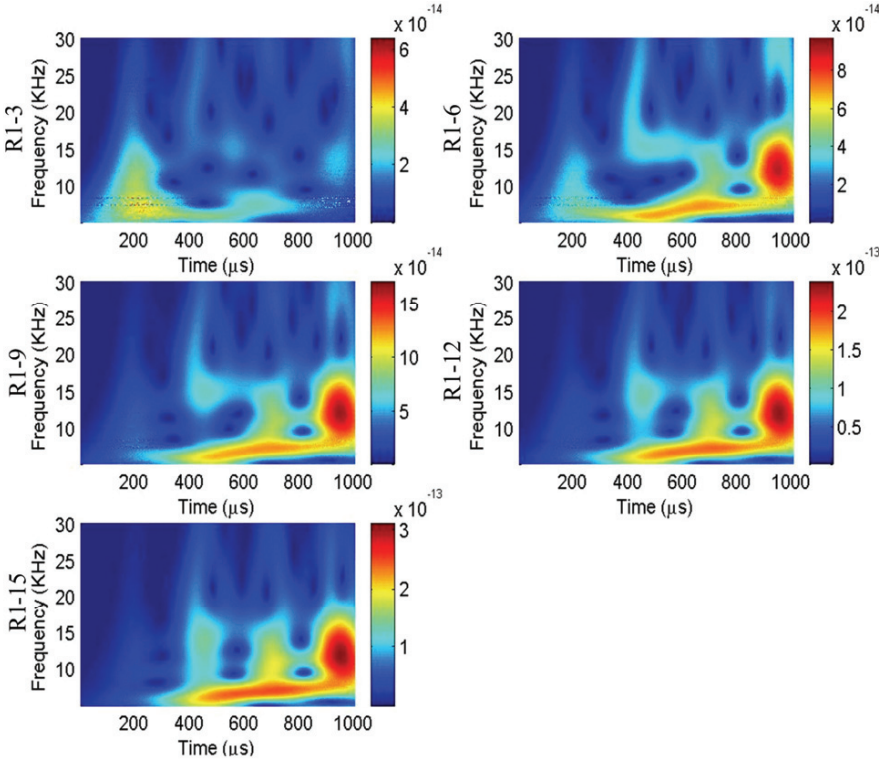

Figure 12: Improved CWT processing

For a beam with inner or lower hard inclusion (see Fig. 1), the similar calculation is performed, and the CWT results about difference data at point A for inner and lower inclusion are calculated, respectively. All results about hard inclusion detection are shown in Table 4. It is similar to the soft inclusion beam, the improved method has

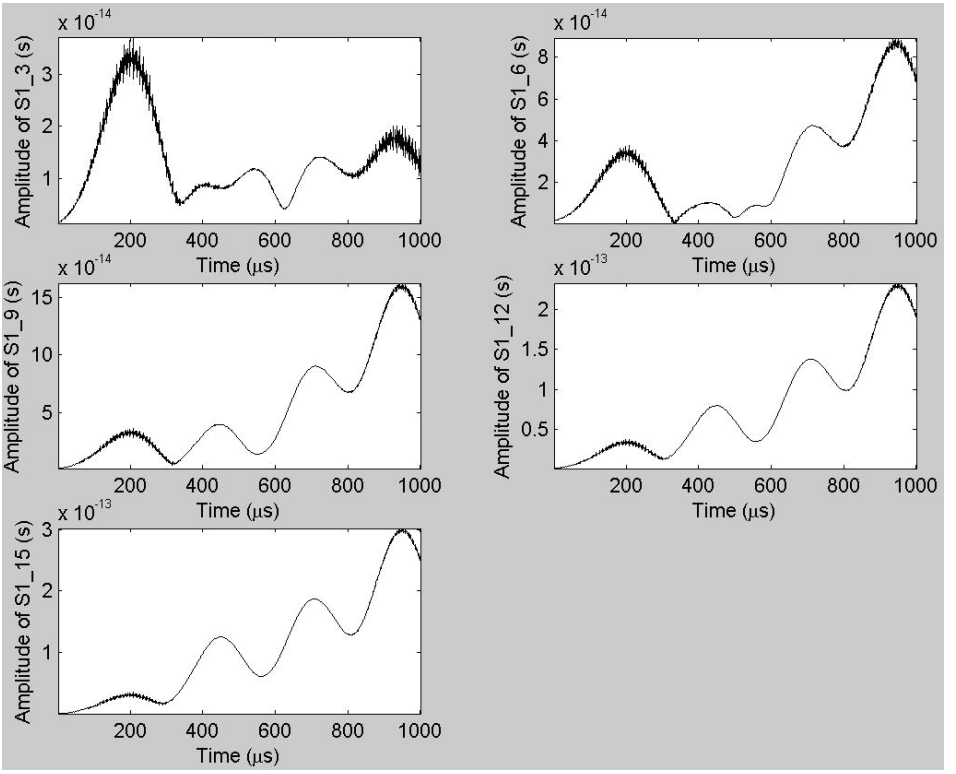

Figure 13: CWT results of point A (11.0 kHz)

a good accuracy for any hard inclusion and it can successfully predict the existence of very small hard inclusion.

4.2 Experiments

Moreover, experiments are carried out to directly measure the dynamic strain signals on the edge of beam. Here, we design a PMMA beam with an upper steel inclusion, where the mechanical properties of materials are the same as listed in Table 3. Since the replicability of impact load is not very convenient to implement experimentally, especially dropping a small ball at a certain height, a moderate inclusion is set 2mm in width, 10mm in length. The typical strain signals measured by strain gauges on points A and B (see Fig. 1) and their CWT results about analysis frequency of 11.0 kHz are both illustrated in Fig. 16. It can be seen in Fig. 16 that the additional ridge reflected by hard inclusion is so evident to diagnose. According to the CWT results in Fig. 16, the location of hard inclusion can be pre-

Table 4: Results of hard inclusion

Hard Inclusion Length (mm)	Inclusion Length Ratio d/h (%)	Upper Inclusion		Inner Inclusion		Lower Inclusion	
		Predicted Location (mm)	Error (%)	Predicted Location (mm)	Error (%)	Predicted Location (mm)	Error (%)
3	9	150.0	0	150.6	0.4	134.5	-10.3
6	19	145.5	-3.0	149.4	-0.4	138.9	-7.4
9	28	150.6	0.4	149.4	-0.4	143.8	-4.1
12	37	148.8	-0.8	150.0	0	146.3	-2.5
15	47	151.8	1.2	150.0	0	146.3	-2.5

dicted successfully but the error can reach to about 11%. In addition, the reflected ratio and transmission ratio of stress wave are separately 38% and 70%. As a result, our detecting method demonstrated experimentally is effective and sensitive to hard inclusion with moderate size in a cantilever beam. If the impact load can be controlled with good replicability by some mechanical ways, the improved method can also be used to detect small hard inclusions.

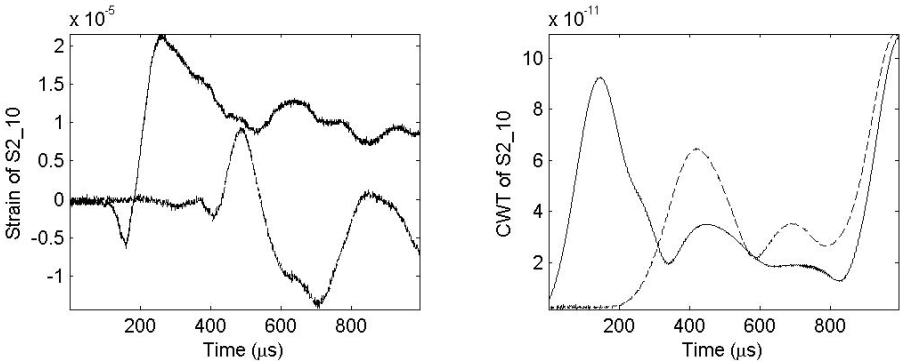

Figure 14: Strain and CWT results of experiment for hard inclusion

5 Conclusion

By Gabor wavelet transform, strain signals has been extracted and analyzed to detect the inhomogeneous character in cantilever beams, and two kinds of inclusions, which are distinct in material properties, have been discussed numerically and experimentally. We predicted the inclusion locations and effects considering three kinds of position of the inclusions in the beams.

For soft inclusion, according to the analysis of FEM numerical computation, when the inclusion depth ratio is larger than 10%, the detecting error in inclusion location is not more than 5%. When the inclusion is very small (d/h<10%), its location can be also successfully identified, though the error will increase. And in experiment, for the soft inclusion depth ratio equal to 32%, the error of prediction is 3.1%, and the same conclusion can be obtained. In addition, considering the reflection or transmission ratios, the extent of soft inclusion can be estimated.

For hard inclusion, it is a little hard to diagnose its existence in beam by former method, so an improved method is proposed to analyze the difference between impure and pure beams by CWT. From calculated results by FEM, when the inclusion depth ratio is larger than 10%, the detecting error in inclusion location is not more

than 10%, and the inclusion size can be evaluated by the CWT results of the differences. In experiment, the normal detection method is carried out for a moderate hard inclusion in beam, and it is sensitive to the inclusion and the error of predicted location is 11%.

All these numerical and experimental results precisely evaluate the location and size of inclusions, especially for soft inclusions, which consequently indicates that the stress wave method based on continuous wavelet transform is a valid and efficient non-destructive detecting method for inhomogeneous inclusion detection. Thus, the method can be expected to expand to a powerful damage detection method in a broad engineering application, especially in inhomogeneous materials and complex structures.

Acknowledgement: The research described here has been supported by the National Natural Science Foundation of China under Grant No. 10672002.

Reference

Baganas K.; Charalambopoulos A.; Manolis G.D. (2005): Detection of spherical inclusions in a bounded elastic cylindrical domain. *Wave Motion*, vol. 41, pp. 13-28.

Brovko A.V.; Murphy E.K.; Rother M.; Yakovlev H.V.V. (2008): Waveguide microwave imaging: spherical inclusion in a dielectric sample. *IEEE Microwave and Wireless Components Letters*, vol. 18, pp. 647-649.

Carreon H. (2007): Thermoelectric detection of hard alpha inclusion in Ti–6Al–4V by magnetic sensing. *Journal of Alloys and Compounds*, vol. 427, pp. 183-189.

Heisenberg W. (1927): Uber den anschaulichen Inhalt der quantentheoretischen Kinematik und Mechanik. *Z. Physik*, vol. 43, pp, 172-198.

Hull A.J.; Hurdis D.A. (2003): A parameter estimation method for the flexural wave properties of a beam. *Journal of Sound and Vibration*, vol. 262, pp. 187-197.

Li Z.; Xia S.; Wang J.; Su X. (2006): Damage detection of cracked beams based on wavelet transform. *International Journal of Impact Engineering*, vol. 32, pp. 1190-1200.

Mallat S. (1998): A Wavelet Tour of Signal Processing. *Academic Press*, New York.

Pidaparti R.M. (2006): Aircraft structural integrity assessment through computational intelligence techniques. *SDHM: Structural Durability & Health Monitoring*, vol. 2, pp. 131-148.

Reddy K.V.; Ganguli R. (2007): Fourier analysis of mode shapes of damaged

beams. *CMC: Computers, Materials, & Continua*, Vol. 5, pp. 79-98.

Tabrez S.; Mitra M.; Gopalakrishnan S. (2007): Modeling of degraded composite beam due to moisture absorption for wave based detection. *CMES: Computer Modeling in Engineering & Sciences*, vol. 22, pp. 77-90.

Tian J.; Gabbert U.; Berger H.; Su X. (2004): Lamb wave interaction with delaminations in CFRP laminates. *CMC: Computers, Materials, & Continua*, vol. 1, pp. 327-336.

Tian J.; Li Z.; Su X. (2003): Crack detection in beams by wavelet analysis of transient flexural waves. *Journal of Sound and Vibration*, vol. 261, pp. 715-727.

Vanaverbeke S.; Leroy O.; Shkerdin G. (2003): Interaction of a bounded ultrasonic beam with a thin inclusion inside a plate. *Journal of the Acoustical Society of America*, vol. 114, pp. 601-610.